Chinese Physics B

PAPER

Interaction of two symmetric monovacancy defects in graphene*

To cite this article: Wen-Yan Xu *et al* 2019 *Chinese Phys. B* **28** 046801

Interaction of two symmetric monovacancy defects in graphene*

Wen-Yan Xu(徐文焱)[1,2], Li-Zhi Zhang(张礼智)[1], Li Huang(黄立)[1], Yan-De Que(阙炎德)[1], Ye-Liang Wang(王业亮)[1], Xiao Lin(林晓)[1], and Shi-Xuan Du(杜世萱)[1,†]

[1] *Institute of Physics & University of Chinese Academy of Sciences, Chinese Academy of Sciences, Beijing* 100190, *China*
[2] *Suzhou Saibao Calibration Technology Co., Ltd., No.* 4, *Baotong Road, Wuzhong District, Suzhou* 215100, *China*

(Received 24 January 2019; revised manuscript received 3 February 2019; published online 5 March 2019)

We investigate the interactions between two symmetric monovacancy defects in graphene grown on Ru (0001) after silicon intercalation by combining first-principles calculations with scanning tunneling microscopy (STM). First-principles calculations based on free-standing graphene show that the interaction is weak and no scattering pattern is observed when the two vacancies are located in the same sublattice of graphene, no matter how close they are, except that they are next to each other. For the two vacancies in different sublattices of graphene, the interaction strongly influences the scattering and new patterns' emerge, which are determined by the distance between two vacancies. Further experiments on silicon intercalated graphene epitaxially grown on Ru (0001) shows that the experiment results are consistent with the simulated STM images based on free-standing graphene, suggesting that a single layer of silicon is good enough to decouple the strong interaction between graphene and the Ru (0001) substrate.

Keywords: monovacancy defect, graphene, density functional theory, STM

PACS: 68.35.Dv, 73.22.Pr, 68.37.Ef, 71.15.–m **DOI:** 10.1088/1674-1056/28/4/046801

1. Introduction

Graphene, carbon in the form of two-dimensional hexagonal lattice, which exhibits amazing optical, electrical, thermal and mechanical properties,[1–5] has become one of the most inspiring research topics since it was discovered in 2004. Because of its high mobility and near-ballistic transport at room temperature,[6] graphene has potential applications in the nanoelectronics. However, these super excellent electronic and transport properties are affected by various defects.[7–10] For example, vacancies, adatoms, Stone-Wales defects, substitutional impurities or topological defects are inevitably formed during the growth of graphene.[11,12] The defects commonly present in graphene are a limiting factor for electronic transport and device performance through charged impurities[13] or resonant scatters.[14] To improve device performance and utilize the full potential of graphene, it is crucial to identify these defects, particularly how they interact with each other and how they affect the electronic properties of graphene.

One of the most common defects in graphene is atomic vacancy, which is expected to be of fundamental importance regarding the electron transport properties of graphene-based devices. Atomic vacancies lead to sharp electronic resonances at the Fermi energy, which significantly limit the mobility of carriers in graphene and can be associated with the formation of local magnetic moments.[15] Recently, the π magnetism of a single carbon vacancy in graphene has been confirmed by using a scanning tunneling microscope.[16] It is known that both the symmetric monovacancy defect and its reconstructed configuration (asymmetric monovacancy) have been found in a graphene system, where the asymmetric configuration is the most stable.[17] The interaction between the asymmetric monovacancy defects in graphene has been investigated by first-principles calculations.[18] However, there is no report about the interaction between the symmetric monovacancy defects in graphene.

2. Experiment

In this paper, by combining first-principles calculations with scanning tunneling microscopy (STM), we investigate the characterization of symmetric monovacancy defects in graphene and their interactions. First-principles calculation results show that when two symmetric monovacancy defects are in the same sublattice of graphene, scattering of each vacancy keep intact at arbitrary distances except when they are neighboring. When two vacancies are in different sublattices, they present new and complex quantum interference patterns. Our experiments on the silicon intercalated graphene on Ru (0001) prove that the interference between two monovacancy defects appears only if they are in the different sublattices.

All our calculations were performed within density functional theory, as implemented in the Vienna *ab-initio* Simulation Package (VASP) with the projector augmented wave (PAW) method.[19,20] Local density approximation (LDA) in the form of Perdew–Zunger was adopted for the exchange-

*Project supported by the National Key Research and Development Program of China (Grant Nos. 2016YFA0202300 and 2018YFA0305800), the National Natural Science Foundation of China (Grant Nos. 61622116, 61474141, 61390501, and 11604373), and the Pioneer Hundred Talents Program, Chinese Academy of Sciences.

†Corresponding author. E-mail: sxdu@iphy.ac.cn

correlation functional.[21] The energy cutoff of the plane-wave basis sets was 300 eV. To confirm the independence of the point defect, a 20×20 supercell of graphene and an 8 Å vacuum layer were used. In our calculations, all the carbon atoms were fixed in the same plane, and they were fully relaxed in geometric optimizations until the residual forces were smaller than 0.02 eV/Å. Due to the calculation limitation, a Gamma point K-sampling was employed to investigate the Brillouin zone matrix. The experimental data were acquired with an ultrahigh-vacuum (UHV) system with a base pressure of 1×10^{-10} mbar (1 bar = 10^5 Pa), which is equipped with an Omicron STM, low energy electron diffraction (LEED), silicon evaporators, and an electron beam heater.[22,23] The Ru (0001) surface has been prepared by argon-ion sputtering and annealing to the 1100 K, and was exposed to oxygen at 1500 K to remove the residual carbon. Monolayer graphene was grown on the surface of Ru (0001) by thermal decomposition of ethylene at 1100 K. Silicon atoms was evaporated to the graphene surface and then annealed at 800 K, producing an intercalated Si layer between the graphene and Ru.[24]

3. Results

In Fig. 1(a), we provide the schematic configuration of a monovacancy defect in free-standing graphene. The calculated density of states projected (PDOS) on the three carbon atoms next to the atomic defect shows a defect state near Fermi level (Fig. 1(e)). When two monovacancy defects are located in graphene, there exist many configurations because of different relative sites of the two vacancies. Here, we focus on three kinds of configurations whose symmetry axes are along the line connecting the two monovacancy defects. The line connecting the two vacancies is parallel to that of carbon-carbon bonds. Figure 1(b) shows the two vacancies located in the same sublattice of graphene (Config A–A). The second configuration is that the left-hand vacancy is located in the B sublattice of graphene, and the right-hand vacancy is in the A sublattice of graphene, as shown in Fig. 1(c) (Config B–A). In the third configuration, the left-hand vacancy is located in the A sublattice of graphene, and the right-hand vacancy is in the B sublattice of graphene (Config A–B, Fig. 1(d)). For these three kinds of configurations, we also calculate the PDOS projected on the three carbon atoms next to each defect. The PDOS of Config A–A has a peak which is similar to that of a single vacancy in graphene (Figs. 1(f) and 1(e), respectively). For Config B–A, the PDOS of the two defects decreases dramatically and the peak moves to the energy below the Fermi energy (Fig. 1(g)). The decrease of the PDOS indicates very strong scattering in this configuration. The PDOS of Config A–B has a similar distribution to that of one vacancy in graphene except a small inflexion on the right-hand side of the peak (Fig. 1(h)).

With these three kinds of configurations, we further change the distance between these two monovacancy defects, and simulate the corresponding STM images (corresponding to the local density of states), where the results are shown in Fig. 2. For Config A–A, at large distances (Figs. 2(c) and 2(d)), the scattering of each defect keeps almost the same as scenario of an isolated vacancy in graphene without new quantum interferences, and the system has only two-fold symmetry. When the distance decreases, new complex interferences exist, especially in the area between the two vacancies (Fig. 2(b)). At the smallest distance (6 times carbon–carbon length between two monovacancy defects) the electronic pattern resumes a well-defined three-fold symmetry (Fig. 2(a)). While for the Config B–A, there are very strong interferences between the two vacancies at different distances (Figs. 2(f)–2(h)). At the smallest distance (4 times carbon-carbon length between the two vacancies) a completely new electronic pattern with twofold symmetry emerges (Fig. 2(e)). For the Config A–B, it is very similar to that of Config B–A, which also has new and complex quantum interference at the varied distances (Figs. 2(j)–2(l)). But in the Config A–B with the smallest distance (5 times carbon-carbon length between the two vacancies), the electron pattern renews a well-defined two-fold symmetry (Fig. 2(i)). Therefore, these data reveal that the interaction between the two vacancies changes dramatically at different distances and configurations, and induces different quantum interferences.

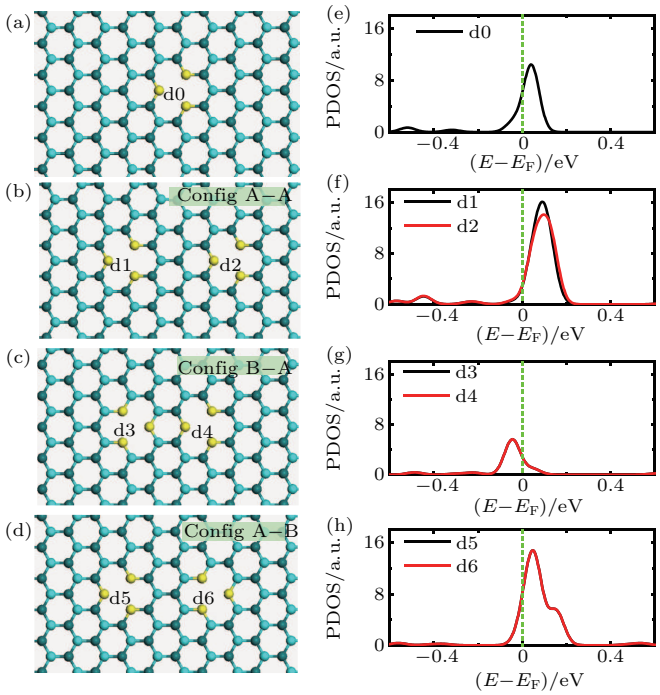

Fig. 1. Atomic configuration of defects in graphene and corresponding PDOS projected on three carbon atoms around monovacancy defects. Grey and cyan atoms correspond to carbon atoms in different sublattices. Yellow atoms are carbon atoms around defect. (a) One single vacancy in graphene. (b) Two vacancies in graphene, which are in the same sublattice of graphene. (c) Two vacancies in graphene: left-hand vacancy is in B sublattice, and right-hand vacancy is in A sublattice. (d) Two vacancies in graphene: left-hand vacancy is in A sublattice, and right-hand vacancy is in B sublattice. (e)–(h) Corresponding PDOS projected on three carbon atoms around monovacancy defect of panels (a)–(d), respectively.

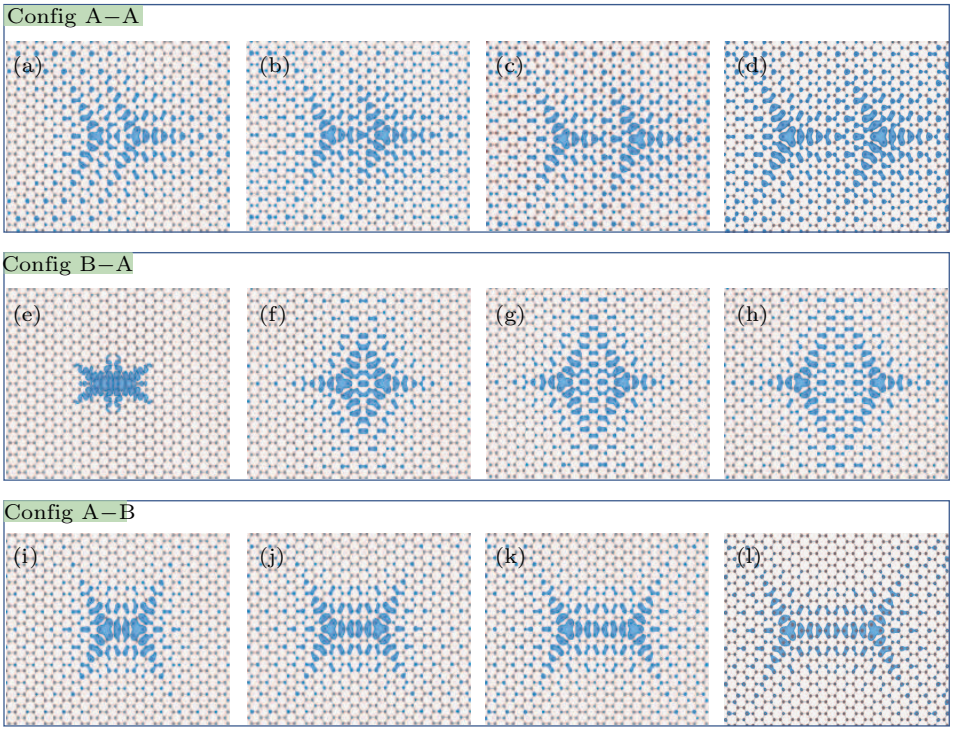

Fig. 2. Simulated STM images of three configurations with two vacancies in graphene. (a)–(d) Configurations shown in Fig. 1(b) with distance of 6, 9, 12, and 15 times carbon–carbon length between the two vacancies, respectively. (e)–(h) Configurations shown in Fig. 1(c) with distances of 4, 7, 10, and 13 times carbon–carbon length between the two vacancies, respectively. (i)–(l) Configurations shown in Fig. 1(d) with distances of 5, 8, 11, and 14 times carbon–carbon length between the two vacancies, respectively.

To confirm our theoretical characterization of vacancies and their interactions, we perform the corresponding experimental characterization of these kinds of vacancies in graphene. Monolayer graphene is grown on the surface of Ru (0001) and then Si layer is intercalated between the graphene and Ru. The intercalated silicon layer has proved to be silicene.[25] This silicene intercalated graphene is decoupled from its substrate as demonstrated by the ARPES measurements, which indicates that the silicene-intercalated graphene possesses the same linear dispersion as that of the free-standing graphene sheet.[24] In our STM results, most regions of the sample exhibit the perfect honeycomb lattice of monolayer graphene, and we could only find a few monovacancy defects. The STM images of the G/Si/Ru containing local defects are shown in Figs. 3(a)–3(c). The most characteristic feature of the defects in Fig. 3(a) is an electronic protrusion involving a complex electronic pattern. Quantum interferences are found in the vicinity of defects, leading to a $(\sqrt{3}\times\sqrt{3})$ R30° superstructure with respect to the graphene (1×1) lattice (R30°). These interferences are assigned to intervalley coupling of graphene π-like states.[26] The Single atomic vacancies are the only well investigated point defects in a graphene system by STM, which shows a characteristic electronic pattern with a well-defined threefold symmetry.[15,27] However, the central part of defects (Fig. 3(a)) is different from that of single atomic vacancies. To reveal unambiguously the atomic structure of the defect here observed, we performed density functional theory (DFT) calculations. The resulting atomic structure is shown in Fig. 1(b), and the two vacancies both are in the A sublattice of graphene. The simulated image obtained from the relaxed structure (Fig. 3(d)) captures the main features of the experimental STM image (Fig. 3(a)). This excellent agreement allows us to unambiguously identify these defects with two neighboring vacancies in the same sublattice. We also investigate the interactions between two monovacancy defects which are both in the same sublattice of graphene at other different distances. Figure 3(b) shows two vacancies at a medium distance. The R30° superstructure is preserved, and quantum interferences induced by each monovacancy defect keep intact at this distance except a simple addition of the local density of states in the overlapping region. The interaction between two monovacancy defects does not produce any new interferences at this distance. The STM image containing two such monovacancy defects with a long enough distance is shown in Fig. 3(c). This shows the characteristic electronic pattern of monovacancy defect, and the interactions between the two vacancies at this distance are negligible. The corresponding DFT simulated images are shown in Figs. 3(e) and 3(f). Due to the restriction of computing capability, the results in Fig. 3(f) are obtained by combining two STM simulations of two separated monovacacy defects. The simulated images accord well with the experimental results. Therefore, we confirm that the interactions between the two monovacancy defects in the same sublattice will not influence quantum interferences induced by each monovacancy defect.

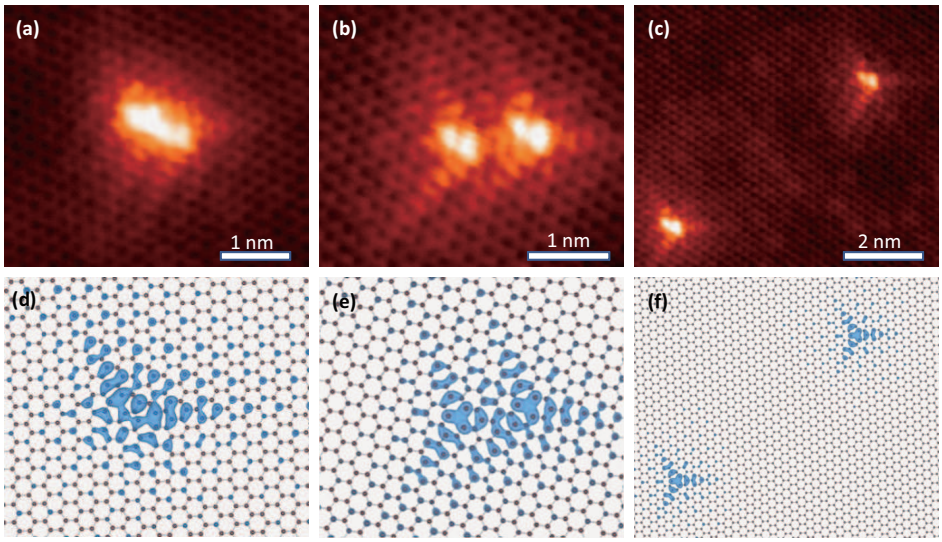

Fig. 3. STM images and corresponding simulated STM images of two vacancies in the same sublattice of graphene with different distances. (a) STM image ($U = -0.8$ V and $I = 0.3$ nA) showing two vacancies at the shortest distance. (b) STM image showing two vacancies at small distance (-0.8 V, 0.4 nA). (c) STM image (-0.8 V, 0.3 nA) showing two vacancies at long distance. (d)–(f) Corresponding simulated STM images of panels (a)–(c), respectively.

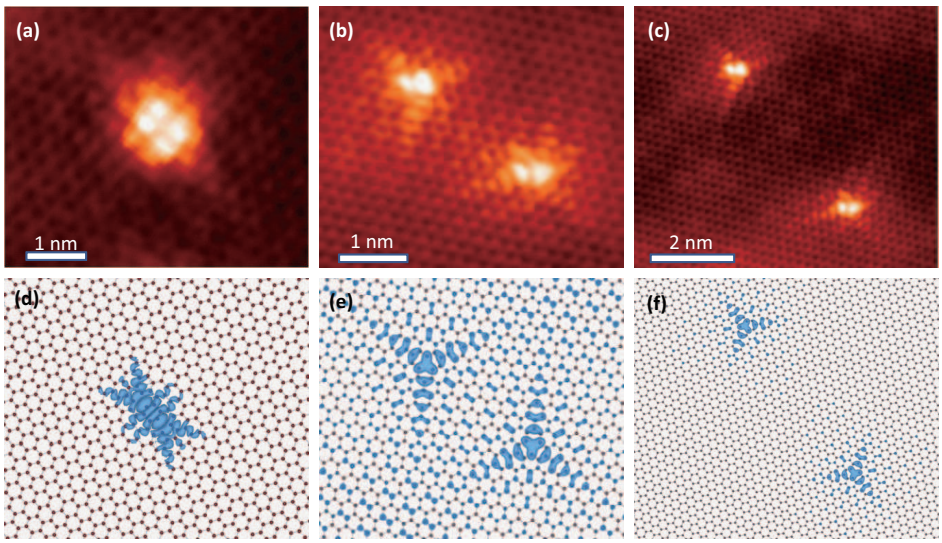

Fig. 4. STM images and corresponding simulated STM images of two vacancies in different sublattices of graphene at different distances. (a) STM image ($U = -0.8$ V and $I = 0.3$ nA) showing two vacancies at the closest distance. (b) STM image showing two vacancies at small distance (-0.8 V, 0.3 nA). (c) STM image (-0.8 V, 0.3 nA) showing two vacancies at long distance. (d)–(f) Corresponding DFT-simulated STM images of panels (a)–(c), respectively.

We also explore the interactions between two monovacancy defects which are in different sublattices by STM. The STM images of these local defects with different sublattices in G/Si/Ru sample are shown in Figs. 4(a)–4(c). These defects are in the form of protrusions with twofold symmetry. Although they have a similar symmetry as divacancy,[28] their centric protrusions are not the same as those of divacancy. Therefore, we perform the DFT calculations to calculate the local density of states of graphene with these defects. The atomic configuration is shown in Fig. 1(c). One vacancy is located in the A sublattice, and the other vacancy is located in the B sublattice of graphene. The distance between the two vacancies is four times the carbon-carbon bond length of graphene. The simulated STM image obtained from the relaxed structure (Fig. 4(d)) has the same twofold symmetry and central protrusions as the experimental STM image (Fig. 4(a)). The excellent agreement allows us to identify these defects with two neighboring monovacancy defects in the different sublattices. From Fig. 4(b), we find that the introduction of two monovacany defects induces new quantum interferences when their distance is small, especially in the area between them. The new complex electronic patterns only exhibit twofold symmetry, which is the same as the corresponding DFT simulated image (shown in Fig. 4(e)). The STM image containing two monovacancy defects with long enough distance is shown in Fig. 4(c). Both of monovacancy defects show a characteris-

tic electronic pattern with a well-defined three-fold symmetry. There are no new quantum interferences between the two monovacancy defects and the interactions between the two vacancy defects can be neglected because of the large distance. The corresponding DFT simulated image is also shown in Fig. 4(f), which accords well with the STM results. Although the configurations A and B shown in Fig. 1(d) are not found in our experiment, we confirm that the interactions strongly influence the scattering when two monovacancy defects are located in different sublattices, and the interactions are also determined by the relative positions and distances between them.

4. Conclusions

In this work, the interactions between two symmetric monovacancy defects in graphene are investigated based on first-principles calculations combined with scanning tunneling microscopy (STM). When the two monovacancy defects are located in the same sublattice of graphene, there are no new states exhibiting. But when the two monovacancy defects are in different sublattices of graphene, the interactions strongly influence the scattering and new patterns exist, which are determined by the relative position and distance between the two monovacancy defects. Our calculation results accord well with the experimental observations on silicene intercalated graphene epitaxially grown on Ru (0001).

Acknowledgment

This work was done in Key Laboratory of Vacuum Physics, Chinese Academy of Sciences.

References

[1] Novoselov K S, Geim A K, Morozov S V, Jiang D, Zhang Y, Dubonos S V Grigorieva I V and Firsov A A 2004 *Science* **306** 666
[2] Castro Neto A H, Guinea F, Peres N M R, Novoselov K S and Geim A K 2009 *Rev. Mod. Phys.* **81** 109
[3] Kim K S, Zhao Y, Jang H, Lee S Y, Kim J M, Kim K S, Ahn J H, Kim P, Choi J Y and Hong B H 2009 *Nature* **457** 706
[4] Balandin A A, Ghosh S, Bao W, Calizo I, Teweldebrhan D, Miao F and Lau C N 2008 *Nano Lett.* **8** 902
[5] Lee C, Wei X, Kysar J W and Hone J 2008 *Science* **321** 385
[6] Du X, Skachko I, Barker A and Andrei E Y 2008 *Nat. Nanotechnol.* **3** 491
[7] Huang L, Xu W Y, Que Y D, Pan Y, Gao M, Pan L D, Guo H M, Wang Y L, Du S X and Gao H J 2012 *Chin. Phys. B* **21** 088102
[8] Huang L T, Chen Z, Wang Y X and Lu Y L 2017 *Chin. Phys. B* **26** 103103
[9] Li S and Lv Z T 2017 *Chin. Phys. B* **26** 036303
[10] Yang Y L and Lu Y 2014 *Chin. Phys. B* **23** 106501
[11] Banhart F, Kotakoski J and Krasheninnikov A V 2011 *ACS Nano* **5** 26
[12] Meyer J C Kisielowski C, Erni R, Rossell M D, Crommie M F and Zettl A 2008 *Nano Lett.* **8** 3582
[13] Tan Y W, Zhang Y, Bolotin K, Zhao Y, Adam S, Hwang E H, Das Sarma S, Stormer H L and Kim P 2007 *Phys. Rev. Lett.* **99** 246803
[14] Ni Z H, Ponomarenko L A, Nair R R, Yang R, Anissimova S, Grigorieva I V, Schedin F, Blake P, Shen Z X, Hill E H, Novoselov K S and Geim A K 2010 *Nano Lett.* **10** 3868
[15] Ugeda M M, Brihuega I, Guinea F and Go'mez-Rodr'guez J M 2010 *Phys. Rev. Lett.* **104** 096804
[16] Zhang Y, Li S Y, Huang H Q, Li W T, Qiao J B, Wang W X, Yin L J, Bai K K, Duan W H and He L 2016 *Phys. Rev. Lett.* **117** 116801
[17] Robertson W, Barbara Montanari, Kuang He, Allen S, Yimin Wu, Harrison M, Kirkl I and Warner H 2013 *ACS Nano* **7** 4495
[18] Zhiming Shi and Udo Schwingenschlögl 2017 *JPCC* **121** 2459
[19] Vanderbilt D 1990 *Phys. Rev. B* **41** 7892
[20] Kresse G and Furthmuller J 1996 *Phys. Rev. B* **54** 11169
[21] Perdew J P, Burke K and Ernzerhof M 1996 *Phys. Rev. Lett.* **77** 3865
[22] Pan Y, Shi D X and Gao H J 2007 *Chin. Phys. B* **16** 3151
[23] Pan Y, Zhang H, Shi D, Sun J, Du S, Liu F and Gao H J 2009 *Adv. Mater.* **21** 2777
[24] Mao J, Huang L, Pan Y, Gao M, He J, Zhou H, Guo H, Tian Y, Zou Q, Zhang L, Zhang H, Wang Y, Du S, Zhou X, Castro Neto A H and Gao H J 2012 *Appl. Phys. Lett.* **100** 093101
[25] Li G, Zhang L, Xu W, Pan J, Song S, Zhang Y, Zhou H, Wang Y, Bao L, Zhang Y, Du S, Ouyang M, Pantelides S and Gao H J 2018 *Adv. Mater.* **30** 1804650
[26] Mallet P, Varchon F, Naud C, Magaud L, Berger C and Veuillen J Y 2007 *Phys. Rev. B* **76** 041403
[27] Kelly K F, Sarkar D, Hale G D, Oldenburg S J and Halas N J 1996 *Science* **273** 1371
[28] Ugeda M M, Brihuega I, Hiebel F, Mallet P, Veuillen J Y, Go'mez-Rodr'guez J M and Yndur'ain F 2012 *Phys. Rev. B* **85** 121402